Proceedings of the 11th Brazilian Congress of Thermal Sciences and Engineering -- ENCIT 2006
Braz. Soc. of Mechanical Sciences and Engineering -- ABCM, Curitiba, Brazil, Dec. 5-8, 2006

Paper CIT06-0983

A NUMERICAL PARAMETRIC STUDY OF A CYLINDRICAL NON-TAPERED AXIALLY ROTATING POROUS HEAT PIPE

Luís Edson Saraiva
Universidade de Passo Fundo – Faculdade de Engenharia e Arquitetura – Campus I – Bairro São José – Caixa Postal 611/631 – Passo Fundo – RS – 99001-970
saraiva@upf.br

Kamal Abdel Radi Ismail
Universidade Estadual de Campinas – Faculdade de Engenharia Mecânica - Cidade Universitária Zeferino Vaz- Rua Mendeleiev, 20 – Caixa Postal 6122 – Campinas – SP - 13083-860
kamal@fem.unicamp.br

Abstract. *This paper presents a model for a two-dimensional axially symmetric rotating heat pipe of cylindrical geometry (non-tapered) and having a porous wick. The model is based upon the conservation of mass, momentum end energy equations. The coupled equations are solved simultaneously by using the finite control volume approach and the SIMPLE algorithm. The model and results are validated by comparison with available results. Simulations were realized to investigate the effects of variation of the rotational speed and the heat flux imposed at the evaporator section on the axial, radial and tangential velocity fields, the pressure and the shear stress distributions. The results indicated the presence of reverse flow as a result of high rotational speeds and heat transfer rates and a reduction of the pumping pressure which ultimately can lead to the dry out of the heat pipe.*

Keywords.*: rotating heat pipe, porous wick*

1. Introduction

Heat pipes are heat transfer elements usually designed to transport high heat transfer rates for long distances with small temperature drop and no external pumping work. Rotating heat pipes, (Gray, 1969), are different from the conventional static heat pipes by their rotation around their own axis or an external axis and are mostly used for cooling electric motors, generators, bearings and many other rotating elements such as turbines and truck breaking systems.

A great deal of the reported work is related to conical rotating heat pipes where the axial component of the centrifugal force helps to return the condensate to the evaporator. The pioneer work of Daniels and Al-Jumaily, (1975) on rotating heat pipes, based on Nusselt model of condensation, was followed by a large number of experimental and analytical investigations based upon their work (Daniels and Williams, 1978 and 1979; Daniels and Al-Baharnah, 1978; Marto, 1976 and Li *et al*., 1993). Later, Ponnappan (1998) showed that the use of Nusselt model of condensation is inadequate for high rotational velocities of the order of 30,000 rpm.

Ismail and Miranda (1997) and Miranda (1989) studied a rotating cylindrical heat pipe with a porous wick and also the case of a rotating wickless heat pipe with conical condenser. They adopted for both cases a two-dimensional model based upon the momentum, energy and mass conservation equations. The authors presented their results of the pressure, velocity and temperature fields in terms of heat transfer rates and the rotational speed. The numerical solution indicated the presence of a region of reverse vapor flow which increased with the increase of the rotational speed. These results were confirmed by Faghri *et al*. (1993) where they solved the vapor region only, and by Harley and Faghri (1995), where they solved the liquid and vapor regions but for a conical heat pipe.

Rotating heat pipes with other geometries were also investigated as the case of a rotating heat pipe with cylindrical stepped wall (Lin, 1991; Lin and Faghri, 1997), constant diameter wickless heat pipe (Lin and Faghri, 1997; Lin and Groll, 1996), finned heat pipes (Marto and Wanniarachchi, 1987; Salinas and Marto, 1991) and miniature heat pipes (Lin and Faghri, 1997).

This paper presents a two dimensional model for the flow and heat transfer in a non tapered rotating heat pipe of plain cylindrical geometry and with a porous wick. The model is based upon the two dimensional equations of conservation of mass, momentum and energy. The equations were solved simultaneously by the finite control volume and the SIMPLE algorithm. The results of the velocity and pressure fields are presented in terms of the rotational speed and heat transfer rates. Extended results can be found in Saraiva (2004).

2. Formulation of the problem

The general geometry of the rotating heat pipe under consideration is shown in Fig. (1). As can be seen, the heat pipe is composed of a plain cylinder fitted with a porous wick, rotating about its own axis, with heat added at one end $\dot{q}$ and removed at the opposite end $-\dot{q}$ while $\dot{m}_l$ and $\dot{m}_v$ denote the liquid and vapor mass flow rates, respectively.

Assuming that the flow is two-dimensional with axial symmetry, steady and compressible in the vapor region and incompressible in the liquid region, with viscous dissipation and constant physical properties, the conservation equations, written for an inertial coordinate system, are shown below. The equations for the porous region were based on the work of Vafai and Tien (1981).

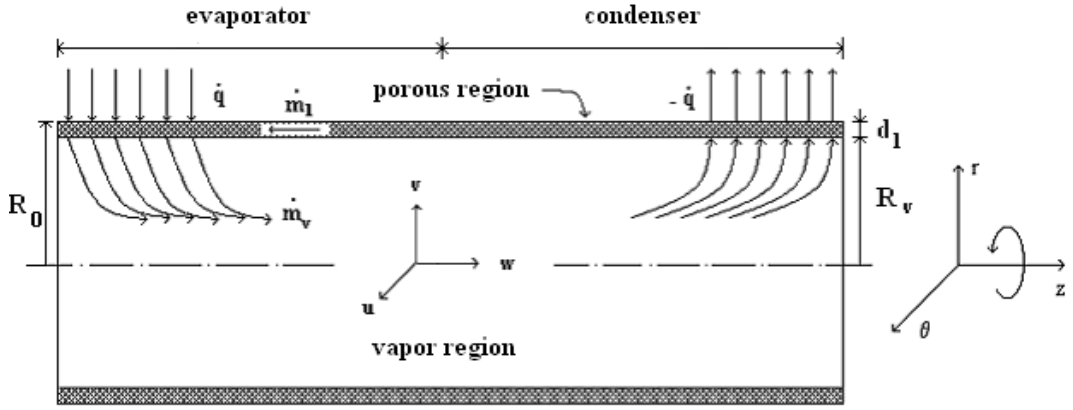

Figure 1. Rotating heat pipe with a porous wick.

2.1. The vapor region

2.1.1. Mass conservation

$$\frac{1}{r}\frac{\partial}{\partial r}\left(r\rho_v v_v\right)+\frac{\partial\left(\rho_v w_v\right)}{\partial z}=0 \tag{1}$$

2.1.2. Momentum along the radial direction

$$\rho_v\left(v_v\frac{\partial v_v}{\partial r}-\frac{u_v^2}{r}+w_v\frac{\partial v_v}{\partial z}\right)=-\frac{\partial p_v}{\partial r}+\mu_v\left(\frac{\partial}{\partial \mathrm{r}}\left(\frac{1}{r}\frac{\partial}{\partial r}\left(rv_v\right)\right)+\frac{\partial^2 v_v}{\partial z^2}\right)$$
$$+\frac{1}{3}\mu_v\left(\frac{\partial}{\partial r}\left(\frac{1}{r}\frac{\partial\left(rv_v\right)}{\partial r}\right)+\frac{\partial^2 w_v}{\partial z\partial r}\right)+2\rho_v\Omega u_v+\rho_v\Omega^2 r \tag{2}$$

where Ω is the rotational speed.

2.1.3. Momentum along the tangential direction

$$\rho_v\left(v_v\frac{\partial u_v}{\partial r}-\frac{v_v u_v}{r}+w_v\frac{\partial u_v}{\partial z}\right)=\mu_v\left(\frac{\partial}{\partial r}\left(\frac{1}{r}\frac{\partial}{\partial r}\left(ru_v\right)\right)+\frac{\partial^2 u_v}{\partial z^2}\right)-2\rho_v\Omega v_v \tag{3}$$

2.1.4. Momentum along the axial direction

$$\rho_v\left(v_v\frac{\partial w_v}{\partial r}+w_v\frac{\partial w_v}{\partial z}\right)=-\frac{\partial p_v}{\partial z}+\mu_v\left(\frac{1}{r}\frac{\partial}{\partial r}\left(r\frac{\partial w_v}{\partial r}\right)+\frac{\partial^2 w_v}{\partial z^2}\right)+\frac{1}{3}\mu_v\left(\frac{\partial^2 w_v}{\partial z^2}+\frac{1}{r}\frac{\partial v_v}{\partial z}+\frac{\partial^2 v_v}{\partial z\partial r}\right) \tag{4}$$

2.1.5. Energy conservation

$$\rho_v c_{p_v}\left(v_v\frac{\partial T_v}{\partial r}+w_v\frac{\partial T_v}{\partial z}\right)=k_v\left(\frac{1}{r}\frac{\partial}{\partial r}\left(r\frac{\partial T_v}{\partial r}\right)+\frac{\partial^2 T_v}{\partial z^2}\right)+v_v\frac{\partial p_v}{\partial r}+u_v\frac{\partial p_v}{\partial z}+\mu\Phi \tag{5}$$

where

$$\Phi = 2\left[\left(\frac{\partial v_v}{\partial r}\right)^2 + \left(\frac{v_v}{r}\right)^2 + \left(\frac{\partial w_v}{\partial z}\right)^2\right] + \left(\frac{\partial u_v}{\partial r} - \frac{u_v}{r}\right)^2 + \left(\frac{\partial u_v}{\partial z}\right)^2 + \left(\frac{\partial v_v}{\partial z} + \frac{\partial w_v}{\partial r}\right)^2 - \frac{2}{3}\left(\frac{\partial v_v}{\partial r} + \frac{v_v}{r} + \frac{\partial w_v}{\partial z}\right)^2 \tag{6}$$

2.2. The liquid region

2.2.1. Mass conservation

$$\frac{1}{r}\frac{\partial}{\partial r}(r v_l) + \frac{\partial w_l}{\partial z} = 0 \tag{7}$$

2.2.2. Momentum along the radial direction

$$\rho_l\left(v_l\frac{\partial v_l}{\partial r} - \frac{u_l^2}{r} + w_l\frac{\partial v_l}{\partial z}\right) = -\varepsilon\frac{\partial p_l}{\partial r} + \mu_l\left(\frac{\partial}{\partial r}\left(\frac{1}{r}\frac{\partial}{\partial r}(r v_l)\right) + \frac{\partial^2 v_l}{\partial z^2}\right) - \frac{\mu_l\varepsilon}{K}v_l + 2\rho_l\Omega u_l + \rho_l\Omega^2 r \tag{8}$$

where ε is the porosity of the porous region and K is its permeability.

2.2.3. Momentum along the tangential direction

$$\rho_l\left(v_l\frac{\partial u_l}{\partial r} - \frac{v_l u_l}{r} + w_l\frac{\partial u_l}{\partial z} - \frac{\mu_l\varepsilon}{K}u_l - 2\rho_l\Omega v_l\right) = \mu_l\left(\frac{\partial}{\partial r}\left(\frac{1}{r}\frac{\partial}{\partial r}(r u_l)\right) + \frac{\partial^2 u_l}{\partial z^2}\right) \tag{9}$$

2.2.4. Momentum along the axial direction

$$\rho_l\left(v_l\frac{\partial w_l}{\partial r} + w_l\frac{\partial w_l}{\partial z}\right) = -\varepsilon\frac{\partial p_l}{\partial z} + \mu_l\left(\frac{1}{r}\frac{\partial}{\partial r}\left(r\frac{\partial w_l}{\partial r}\right) + \frac{\partial^2 w_l}{\partial z^2}\right) - \frac{\mu_l\varepsilon}{K}w_l \tag{10}$$

2.2.5. Energy conservation

$$\rho_l c_{p_l}\left(v_l\frac{\partial T_l}{\partial r} + w_l\frac{\partial T_l}{\partial z}\right) = \frac{k_{eff}}{\varepsilon}\left(\frac{1}{r}\frac{\partial}{\partial r}\left(r\frac{\partial T_l}{\partial r}\right) + \frac{\partial^2 T_l}{\partial z^2}\right) + v_l\frac{\partial p_l}{\partial r} + u_v\frac{\partial p_l}{\partial z} + \mu_l\Phi \tag{11}$$

where k_{eff} is the effective thermal conductivity of the porous medium and Φ is the viscous dissipation term.

$$\Phi = 2\left[\left(\frac{\partial v_l}{\partial r}\right)^2 + \left(\frac{v_l}{r}\right)^2 + \left(\frac{\partial w_l}{\partial z}\right)^2\right] + \left(\frac{\partial u_l}{\partial r} - \frac{u_l}{r}\right)^2 + \left(\frac{\partial u_l}{\partial z}\right)^2 + \left(\frac{\partial v_l}{\partial z} + \frac{\partial w_l}{\partial r}\right)^2 - \frac{2}{3}\left(\frac{\partial v_l}{\partial r} + \frac{v_l}{r} + \frac{\partial w_l}{\partial z}\right)^2 \tag{12}$$

The coupling between the momentum and energy equations is realized by using the state equation.

2.3. The boundary conditions

At the extremities of the heat pipe, ($z = 0, L$), the no-slip condition is used for the conservation of momentum and mass while the adiabatic condition is used for the energy equation, and the conditions can be written as

$$u_{v,l} = v_{v,l} = w_{v,l} = 0 \tag{13}$$

$$\frac{\partial T_{v,l}}{\partial z} = 0 \tag{14}$$

On the symmetry axis, $r = 0$, the radial and tangential velocities are zero and also the radial gradients of the vapor axial velocity and the temperature

$$u_v = v_v = 0 \tag{15}$$

$$\frac{\partial w_v}{\partial r} = 0 \tag{16}$$

$$\frac{\partial T_v}{\partial r} = 0 \tag{17}$$

To couple the vapor region to the porous region, an energy balance is realized along the liquid-vapor interface, $r = R_v$.

$$v_l(z) = \frac{\dot{q}''(z) + k_v \left.\frac{\partial T_v}{\partial r}\right| r = R_v}{\rho_l \lambda} \tag{18}$$

Where $\dot{q}''(z)$ is the local heat flux density at the interface.

The mass conservation at the interface is realized by a mass balance at $r = R_v$

$$v_v(z) = \frac{\rho_l v_l(z)}{\rho_v} \varepsilon \tag{19}$$

The no-slip condition along the liquid-vapor interface ($r = R_v$) is written in terms of the tangential and axial components of velocity

$$u_{v,l} = w_{v,l} = 0 \tag{20}$$

Since the phase change takes place without temperatures drop, one can write at $r = R_v$

$$T_l = T_v \tag{21}$$

that is, the liquid temperature is equal to the saturation temperature at the local vapor pressure.

On the external surface of tube, $r = R_0$, the boundary conditions depend on the axial position along the tube and the mechanism of the local heat transfer. In the present work boundary conditions of the second type are adopted for the evaporator and condenser, respectively

$$k_{ef} \frac{\partial T_l}{\partial r} = \dot{q}'' \tag{22}$$

$$-k_{ef} \frac{\partial T_l}{\partial r} = \dot{q}'' \tag{23}$$

Also, the no-slip condition is imposed on the external surface of the tube ($r = R_0$)

$$u_l = v_l = w_l = 0 \tag{24}$$

3. The numerical treatment

The conservation equations of mass, momentum and energy are solved simultaneously in the vapor and liquid regions by the method of finite control volumes and the SIMPLE algorithm (Patankar, 1980). Numerical tests realized in order to optimize the grid size indicated that 60 control volumes along the axial direction and 17 control volumes along the radial direction are adequate for the vapor region. The grid size for the porous region is found to be 60 × 5.

To validate the numerical scheme the results are compared with available results of Faghri et al. (1993) for a rotating heat pipe having an evaporator length of 0.2 m, adiabatic section of 0.6 m, condenser of 0.2 m and diameter

0.02 m, filled with water vapor at 100ºC. Figure (2) shows the dimensionless axial velocity for $\mathrm{Re}_r = 4$ and different rotational speeds. Figure (3) shows the radial velocity component. As can be seen the results have the same general tendencies, and are in good agreement over the whole range of rotational speeds.

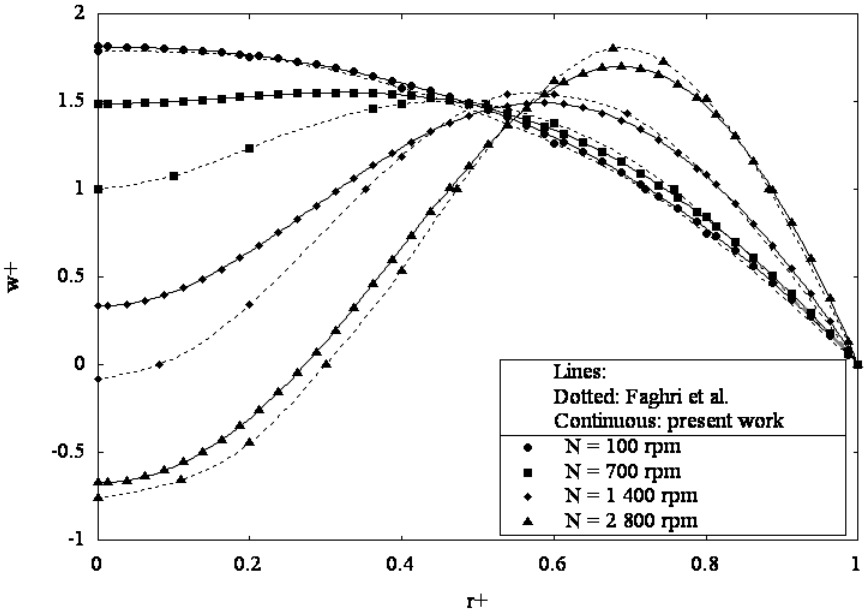

Figure 2. Comparison between the predicted normalized axial velocity at mid point of the evaporator and the results of Faghri et al. (1993).

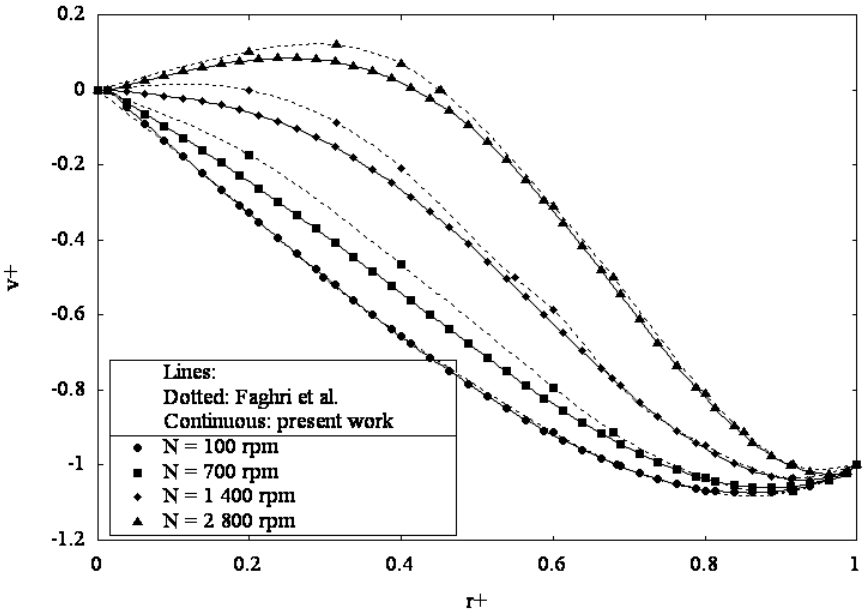

Figure 3. Comparison between the predicted normalized radial velocity at mid point of the evaporator and the results of Faghri et al. (1993).

4. Results and discussion

The numerical simulations were realized for a heat pipe having total length of 1.0 m divided equally between the evaporator and condenser with no adiabatic section and having a porous wick of sintered bronze particles of diameters of 6.83×10^{-4} m, wick thickness of 7.3×10^{-3} m and having water as a working fluid.

The effects of the rotational speed on the axial velocity profiles in the vapor region are shown in Fig. (4). As can be seen the rotational speed moves the region of maximum velocity from the tube center towards the interface near the wall region. Also one can observe the presence of reverse flow which increases with of the rotational speed.

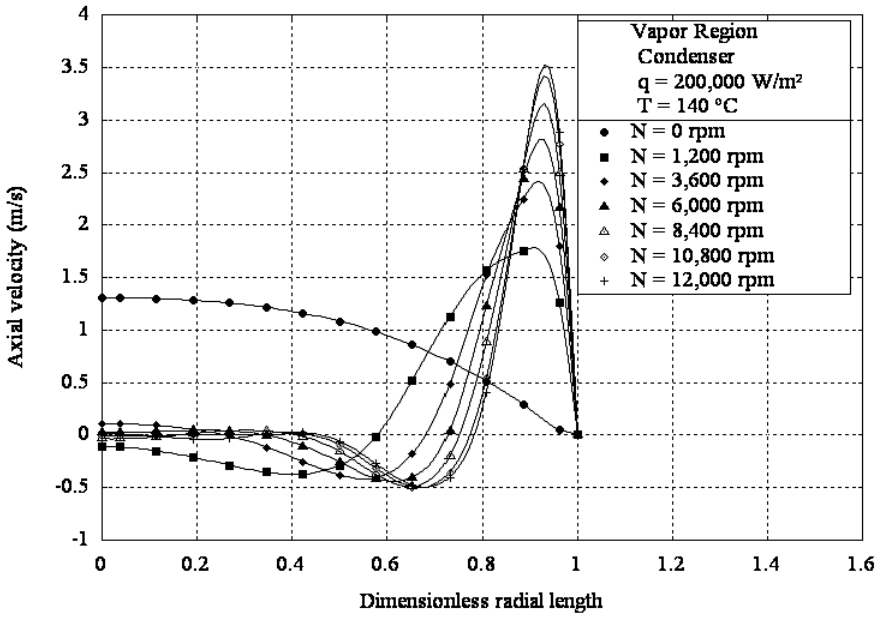

Figure 4. Axial velocity profiles along the radial direction, in the vapor region, at mid point of the condenser, as a function of rotational speed.

The axial velocity in the porous region is fairly sensitive to the variations in the rotational speed as can be deduced from comparing Fig. (5) and Fig. (6). One can observe that the increase of the rotational speed leads to increasing the velocities near the liquid-vapor interface and reducing their values near the wall region. This is because the mass exchange is mainly occurring at the interface while near the wall region the centrifugal force is relatively large and opposing the liquid movement. The radial and tangential components of the velocity are nearly insensitive to the rotational speed in the porous region and hence their corresponding figures are omitted here.

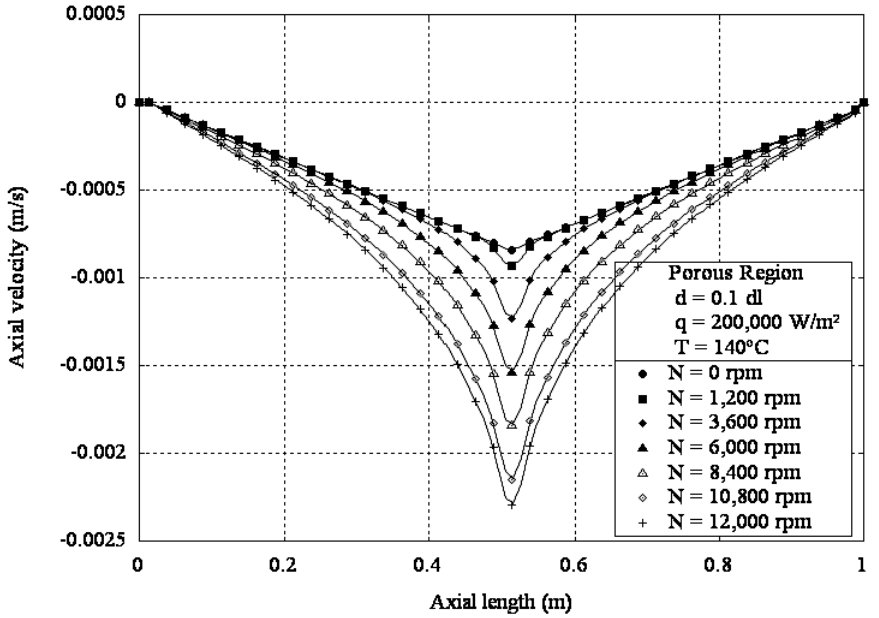

Figure 5. Axial velocity profiles along the axial direction, in the porous region, at a distance from the interface equal to 10% of the porous wick thickness, as a function of rotational speed.

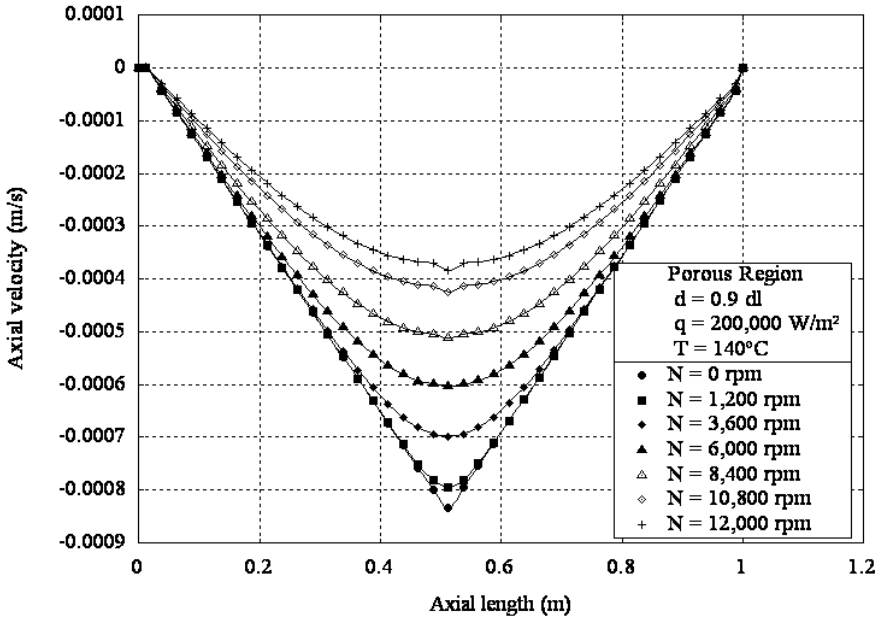

Figure 6. Axial velocity profiles along the axial direction, in the porous region, at a distance from the interface equal to 90% of the porous wick thickness, as a function of rotational speed.

Figure (7) shows the variations of the radial velocity along the tube axis with the rotational speed. The effect of the rotational speed on the direction of the radial velocity can be illustrated by comparing the velocity profiles with those obtained only due to heat transfer ($N = 0$ rpm), showing positive velocities in the evaporator. Similar results, just with negative velocities in the condenser, are omitted here for brevity.

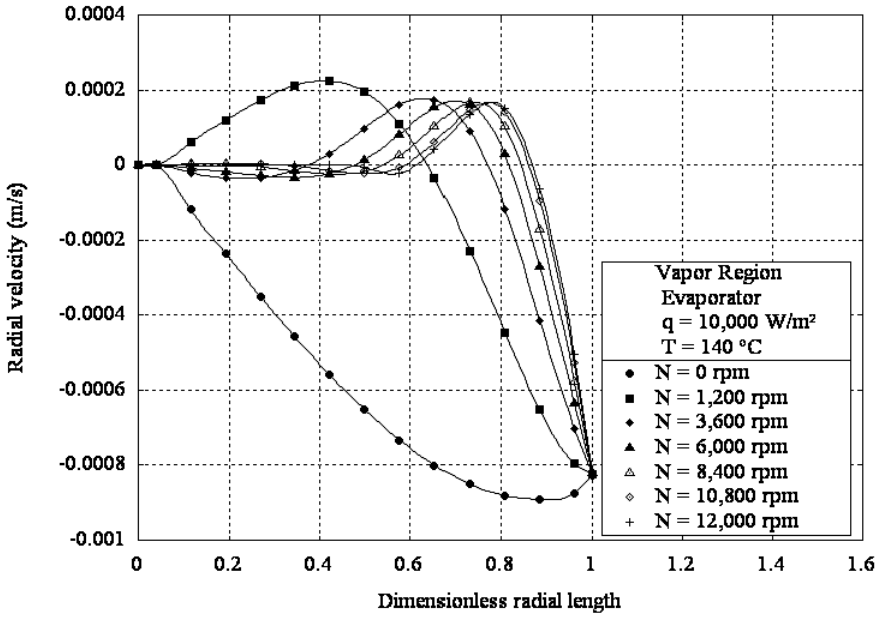

Figure 7. Radial velocity profiles along the radial direction, in the vapor region, at mid point of the evaporator, as a function of rotational speed.

The tangential velocity in the vapor region is strongly affected by the rotational speed as can be deduced from the comparison with the case of $N = 0$ rpm in Fig. (8). As can be seen the effect of increasing the rotational speed is to increase the tangential velocity and displace the region of maximum velocity towards the wall region as a result of the centrifugal forces. Similar results can be found in the case of the condenser, and are omitted here for brevity.

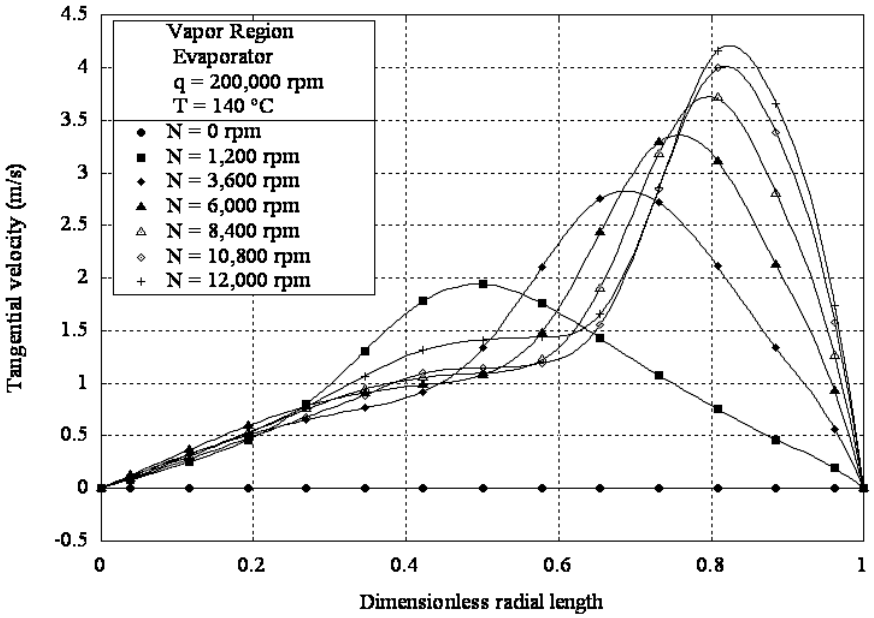

Figure 8. Tangential velocity profiles along the radial direction, in the vapor region, at mid point of the evaporator, as a function of rotational speed.

If one defines the excess pressure term representing as the difference between the maximum capillary pressure and the difference of the local pressure at the interface, this term can be written as

$$p_{ex}(z) = \frac{2\sigma}{r_c} - \left(p_v(z) - p_l(z)\right) \tag{25}$$

Figure (9) shows that the increase of the rotational speed reduces the excess pressure, due to the dominant effect of the centrifugal force on the liquid region because of its higher density in relation to the vapor. As a possible consequence, an eventual excess pressure dropping to zero could prevent the liquid return, leading to drying out the heat pipe.

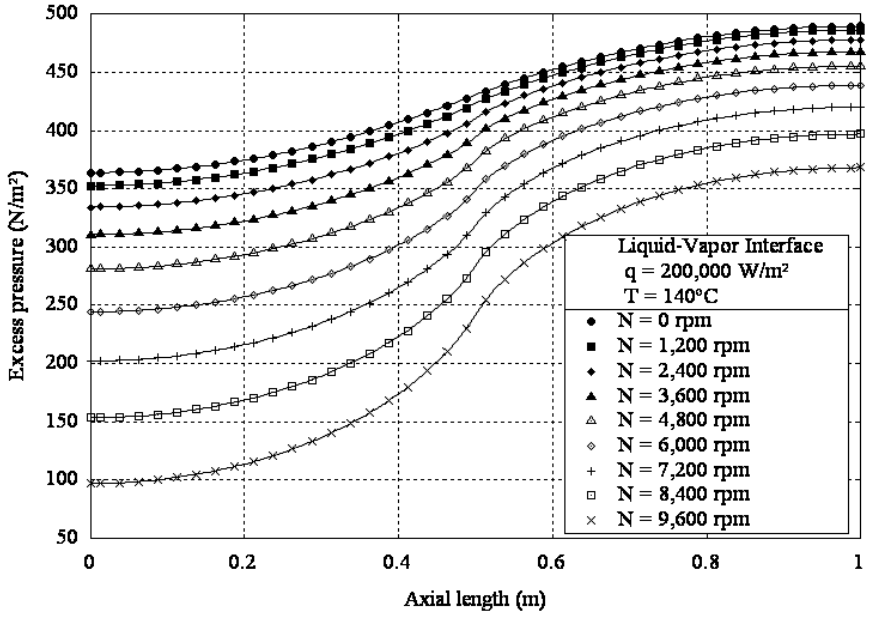

Figure 9. Excess pressure profiles along the axial axis, on the liquid-vapor interface, as a function of rotational speed.

The shear stress at the liquid-vapor interface in the $r\theta$ plane can be written as

$$\tau_{r\theta} = \mu_v \left[r \frac{\partial}{\partial r} \left(\frac{u_v}{r} \right) \right] r = R_v \tag{26}$$

Figure (10) shows the increase of the shear stress $\tau_{r\theta}$ with the increase of the rotational speed. A negative value of the shear stress means that the tangential velocity of the vapor is greater than the tangential velocity at the interface.

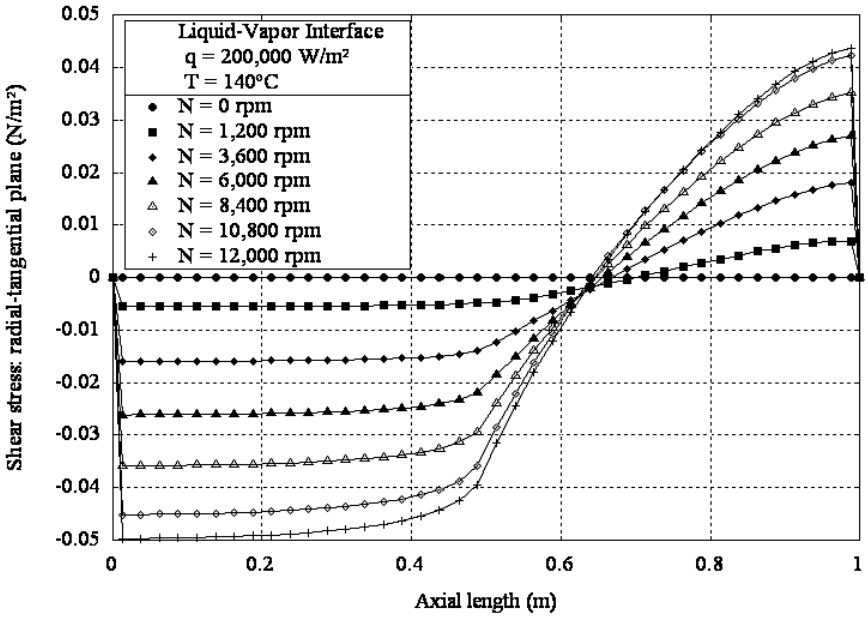

Figure 10. Shear stress profiles along the axial axis, contained in a $r\theta$ plane, on the liquid-vapor interface, as a function of rotational speed.

The shear stress at the interface in the rz plane can be written as

$$\tau_{rz} = \mu_v \left(\frac{\partial w_v}{\partial r} \right) r = R_v \tag{27}$$

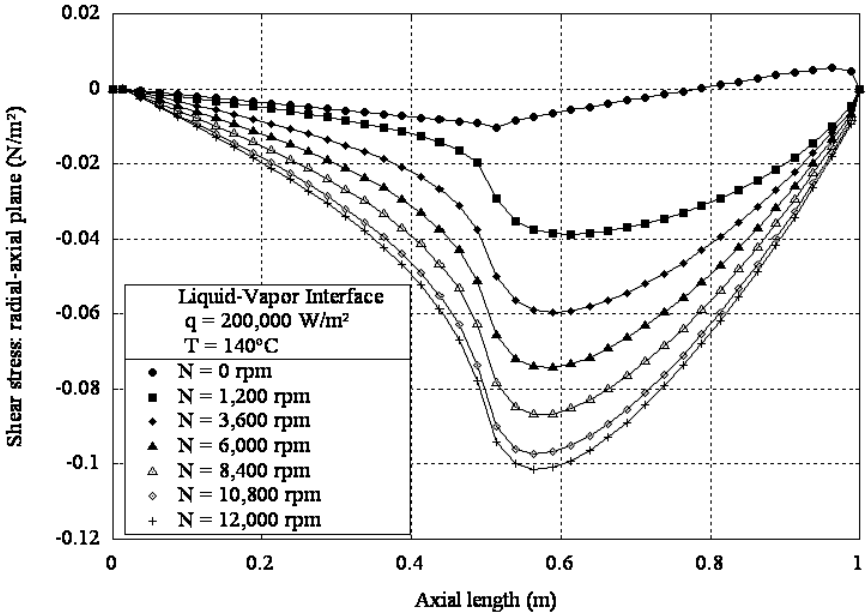

Figure 11. Shear stress profiles along the axial axis, contained in a rz plane, on the liquid-vapor interface, as a function of rotational speed.

Figure (11) shows that the shear stress in the *rz* plane increases with the increase of the rotational speed, which is in agreement with the fact that high axial velocities occur near the interface. Negative values of the shear stress indicate that the vapor axial velocity is greater than the axial velocity at the interface (obeying the no-slip condition).

Figures (12), Fig. (13) and Fig. (14) show the effects of the heat transfer rate on the axial, radial and tangential velocities, respectively. As can be seen, the increase of the heat transfer rate leads to increasing the axial and radial velocity in the condenser and the evaporator as in Fig. (12) and Fig. (13). A similar increase can be seen in the tangential velocity profile as in Fig. (14).

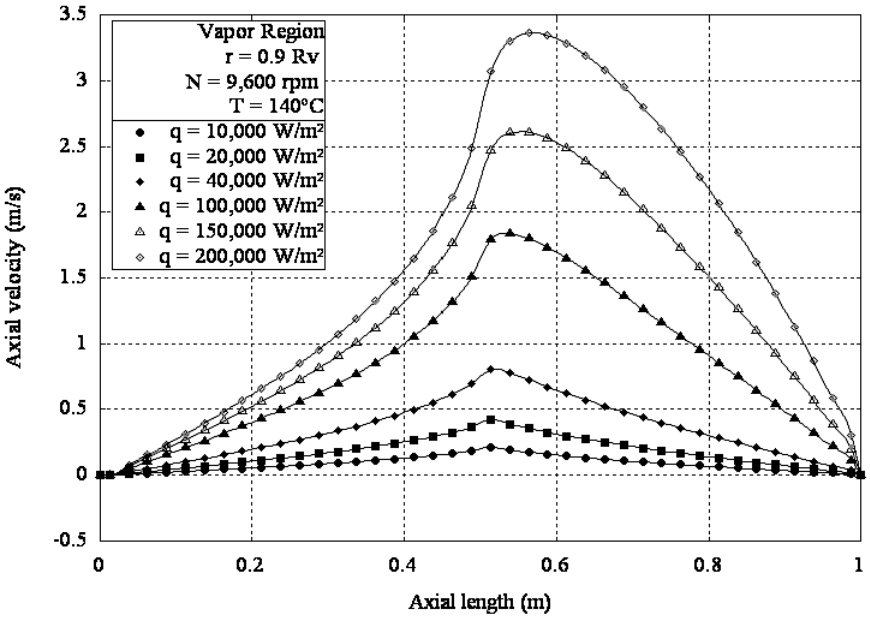

Figure 12. Axial velocity profiles along the axial axis, in the vapor region, at a radius equal to 90% of the vapor medium radius, as a function of heat transfer rates imposed to the evaporator of the heat pipe.

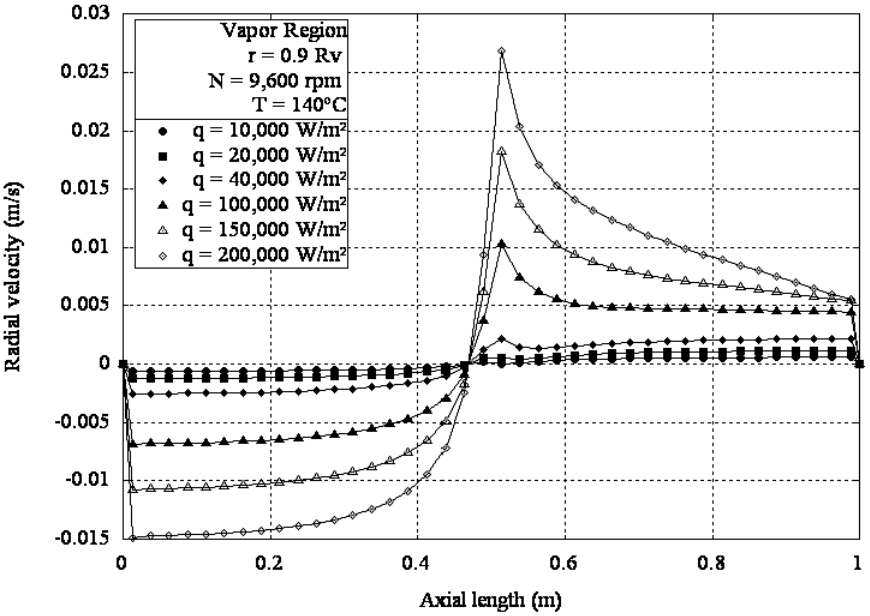

Figure 13. Radial velocity profiles along the axial axis, in the vapor region, at a radius equal to 90% of the vapor medium radius, as a function of heat transfer rates imposed to the evaporator of the heat pipe.

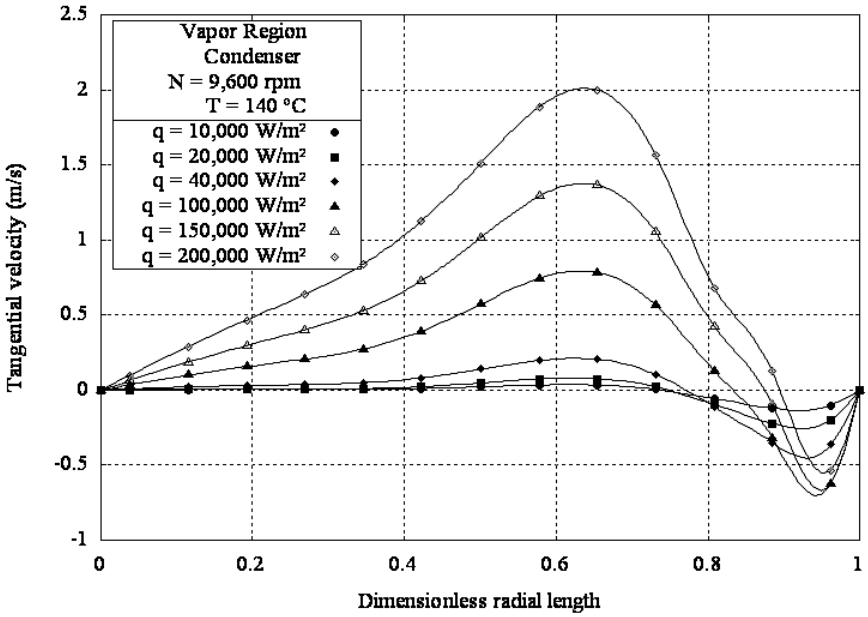

Figure 14. Tangential velocity profiles along the radial axis, in the vapor region, at mid point of the condenser, as a function of heat transfer rates imposed to the evaporator of the heat pipe.

Since the vapor circulation is from the evaporator to the condenser and the liquid circulations is in the opposite direction, the difference $p_v(z) - p_l(z)$, Eq. (25), is greater in the evaporator than in the condenser, implying smaller excess pressures in the first and bigger in the last. Also, greater heat transfer rates require greater fluid circulation and hence bigger pressure difference between the evaporator and the condenser, in both, the vapor and porous regions. The effects of heat transfer rate on the excess pressure (p_{ex}), defined by Eq. (25), are shown in Fig. (14).

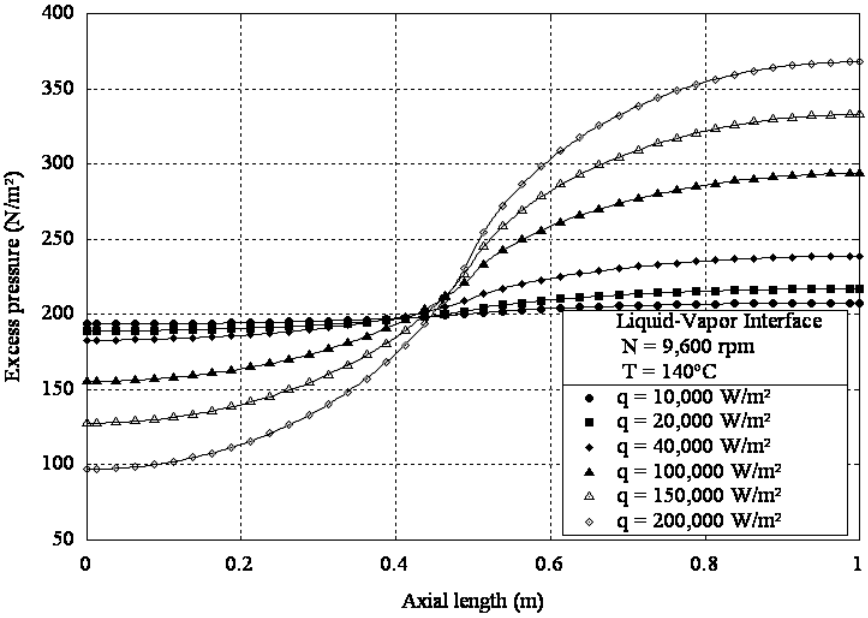

Figure 15. Excess pressure profiles along the axial axis, on the liquid-vapor interface, as a function of heat transfer rates imposed to the evaporator of the heat pipe.

5. Conclusions

This paper presents the results of a two-dimensional axisymmetric model for a rotating heat pipe of cylindrical geometry with a porous wick. The validation of the model is realized by comparison with available results. A parametric study is realized to investigate the effects of the rotational speed and the heat transfer rate on the radial, axial and tangential velocities, the pressure and shear stress distributions. It was found that under certain rotational velocity

conditions, reverse flow could occur. Also, excess pressure at the liquid-vapor interface is sensitive to the rotational speeds as much as to heat transfer rates and its decrease to zero can prevent the liquid return. These conditions can lead to drying out the heat pipe.

6. References

Daniels, T.C. and Al-Jumaily, F.K., 1975, "Investigations of the Factors Affecting the Performance of a Rotating Heat Pipe", International Journal of Heat and Mass Transfer, Vol. 18, pp. 961-973.

Daniels,T.C. and Al-Baharnah, N.S., 1978, "Temperature and Heat Load Distribution in Rotating Heat Pipes, Proceedings of the International Heat Pipe Conference, Vol. 3, pp.170-176.

Daniels,T.C. and Williams,R.J., 1978, "Experimental Temperature Distribution and Heat Load Characteristics of Rotating Heat Pipes", International Journal of Heat and Mass Transfer, Vol. 21, pp. 193-201.

Daniels,T.C. and Williams,R.J., 1979, "The Effect of External Boundary Conditions on Condensation Heat Transfer in Rotating Heat Pipes", International Journal of Heat and Mass Transfer, Vol. 22, pp. 1237-1241.

Faghri, A., Gogineni, S. and Thomas, S., 1993, "Vapor Flow Analysis of an Axially Rotating Heat Pipe", International Journal of Heat and Mass Transfer, Vol. 36, No. 9, pp. 2293-2303.

Gray, V.H., 1969, "The Rotating Heat Pipe; a Wickless, Hollow Shaft for Transferring High Heat Fluxes", Proceedings of the ASME/AIChE Heat Transfer Conference, Minneapolis, pp. 1-5.

Harley, C. and Faghri, A., 1995, "Two-dimensional Rotating Heat Pipe Analysis", Journal of Heat Transfer-Transactions of the ASME, Vol. 117, pp. 202-208.

Ismail, K.A.R. and Miranda, R.F., 1997, "Two-dimensional Axisymmetrical Model for a Rotating Porous Wicked Heat Pipe", Applied Thermal Engineering, Vol. 17, No. 2, pp. 135-155.

Li, H.M., Liu, C.Y. and Damodaran, M., 1993, "Analytical Study of the Flow and Heat Transfer in a Rotating Heat Pipe", Heat Recovery Systems & CHP, Vol. 13, No. 2, pp. 115-122.

Lin, L. and Faghri, A., 1997, "Heat Transfer Analysis of Stratified Flow in Rotating Heat Pipes with Cylindrical and Stepped Walls", International Journal of Heat and Mass Transfer, Vol. 40, No. 18, pp. 4393-4404.

Lin, L. and Faghri, A., 1997, "Steady-State Performance of a Rotating Miniature Heat Pipe", Journal of Thermophysics and Heat Transfer, Vol. 11, No. 4, pp.513-518.

Lin, L. and Groll, M., 1996, "Critical Conditions for Collapse of Annular Flow in a Rotating Heat Pipe with a Cylindrical Wall", Heat Transfer Engineering, Vol. 17, No. 3, pp. 29-34.

Lin, L., 1991, "Cellular Flow in a Rotating Heat Pipe with Stepped Wall", Heat Recovery Systems & CHP, Vol. 11, No. 1, pp. 63-68.

Marto, P.J. and Wanniarachchi, A.S., 1987, "Influence of Internal Axial Fins on Condensation Heat Transfer in Co-axial Rotating Heat Pipes, in: W.-J. Yang, Heat Transfer and Fluid Flow in Rotating Machinery, Hemisphere Publishing Co.

Marto, P.J., 1976, "Performance Characteristics of Rotating, Wickless Heat Pipes, Proceedings of the International Heat Pipe Conference, Vol. 2, pp. 281-291.

Miranda, R. F., 1989, "Desenvolvimento de um Modelo Matemático para a Análise Local do Desempenho de Tubos de Calor com Rotação em seu Eixo Axial", PhD thesis, University of Campinas, Brazil.

Patankar, S.V., 1980, "Numerical Heat Transfer and Fluid Flow", Hemisphere Publishing Corporation, 197 p.

Ponnappan, R. and He, Q., 1998, "Test Results of Water and Methanol High-Speed Rotating Heat Pipes", Journal of Thermophysics and Heat Transfer, Vol. 12, pp. 391-397.

Salinas, D. and Marto, P.J., 1991, "Analysis of an Internally Finned Rotating Heat Pipe", Numerical Heat Transfer, Vol. 19, pp. 255-275.

Saraiva, L. E., 2004, "Simulação Numérica para Análise Local e Global do Desempenho de Tubos de Calor Rotativos com Estrutura Porosa", PhD thesis, University of Campinas, Brazil.

Vafai, K. and Tien, C.L., 1981, "Boundary and Inertia Effects on Flow and Heat Transfer in Porous Media", International Journal of Heat and Mass Transfer, Vol. 24, pp. 195-203.